DOI: 10.13009/EUCASS2022-6065
9TH EUROPEAN CONFERENCE FOR AERONAUTICS AND SPACE SCIENCES (EUCASS)

Minimum-Fuel Orbit Transfers Using Modified Equinoctial Elements via Indirect Heuristic Method

Vincenzo Romano, Francesco Corallo **, Mauro Pontani***, and Paolo Teofilatto*****
** Faculty of Civil and Industrial Engineering, Sapienza Università di Roma*
Via Salaria 851, 00138 Rome, Italy, romano.vincenzo.1997@gmail.com
*** Thales Alenia Space Italia*
Via Saccomuro 24, 00131 Rome, Italy, francesco.corallo@thalesaleniaspace.com
**** Department of Astronautical, Electrical, and Energy Engineering, Sapienza Università di Roma,*
Via Salaria 851, 00138 Rome, Italy, mauro.pontani@uniroma1.it
***** School of Aerospace Engineering, Sapienza Università di Roma,*
Via Salaria 851, 00138 Rome, Italy, paolo.teofilatto@uniroma1.it

Abstract
Minimum-fuel orbit transfers can include an unspecified number of coast arcs and maximum-thrust phases, whose sequence and timing are unknown a priori. The indirect heuristic method is proposed as the numerical solution approach, and applied to an illustrative example already addressed in previous research. The minimum-fuel transfer found in this study outperforms that reported in the scientific literature. Moreover, this research proves that additional locally optimal solutions exist to the same minimum-fuel problem. With different propulsion parameters, the number of coast and thrust arcs changes, and this testifies to the existence of a variety of structures for minimum-fuel orbit transfers.

1. Introduction

Orbit maneuvering represents a crucial task for spacecraft orbiting the Earth or dedicated to the planetary exploration. As the vehicle weight is a crucial issue for space missions, minimization of the propellant consumption required for transferring a spacecraft between two specified orbits is desirable. Minimum-fuel paths have been investigated using a variety of analytical and numerical approaches. Early studies date back to the 1920s with the pioneering work by Hohmann [1], and continued in the subsequent decades. Significant advances are dated back to the 1950s, when also the modern optimal control theory began developing, by gradually assuming its current form, due to the researches of some eminent scientists, such as Bliss [2], Leitmann [3], Cicala [4], Belmann [5], Miele [6], Pontryagin [7], Bryson [8], and Vinh [9]. In the same period Lawden introduced the primer vector theory [10], which is concerned with the application of the first–order necessary conditions for optimality, arising from the calculus of variations. The impulsive thrust assumption [11] represents an excellent approximation for spacecraft that employ chemical propulsion for short durations. However, in the presence of moderate or low thrust levels, the general properties of minimum-fuel finite-thrust paths can no longer be inferred from an impulsive solution [12], and optimal space trajectories must be found as the solutions of a continuous-time optimal control problem. These are not amenable to closed-form or analytical solutions, therefore numerical approaches are mandatory. With this regard, Betts [13] and Conway [14] offer excellent overviews of the available methods in spacecraft trajectory optimization.

The indirect heuristic method (IHM) [15,16] has recently emerged as a hybrid methodology that avoids some major shortcomings of classical numerical optimization methods, such as the need of an appropriate first-attempt approximate solution or the use of a large number of parameters to discretize the problem. IHM is based on the joint use of the analytical conditions for optimality and a heuristic algorithm. The control variables, i.e. thrust magnitude and direction, are expressed in terms of the costate conjugate to the spacecraft equations of motion. This leads to defining a two-point boundary-value problem, which includes a reduced number of unknown parameters, i.e. the time of flight and the unknown initial values of the costate variables. However, usually these are challenging to find, and this task is thus demanded to a heuristic technique, which does not require any starting guess solution. Genetic algorithms (GA), Particle Swarm Optimization (PSO), and Differential Evolution (DE) [17] represent well established heuristic

DOI: 10.13009/EUCASS2022-6065

approaches. In most cases, these methodologies are inspired by natural behaviors or phenomena and aim at implementing the biological principle of survival of the fittest.

As a further complicacy, minimum-fuel paths using finite thrust are associated with a set of necessary conditions that admit coast arcs and powered phases [18]. This consolidated property was proven in the 60s [10] and since then a vast amount of literature was dedicated to investigating minimum-fuel space trajectories. A very interesting recent contribution is due to Taheri and Junkins [12], who analyzed the relations between impulsive transfers and finite-thrust paths using optimal control theory. They point out the existence of optimal trajectories with a variety of structures (i.e. different numbers and timing of powered phases and thrust arcs). In this context, the switching function, which depends on the state and the costate variables, plays a major role. Recently, Pan et al. [19] and Pontani [18] provided the closed-form costate along optimal coast arcs employing spherical coordinates and modified equinoctial elements, respectively.

The work that follows is focused on the numerical detection of minimum-fuel orbit transfers, using modified equinoctial elements (MEE) for orbit dynamics and IHM as the numerical solution technique. The choice of MEE is related to three remarkable properties. First, virtually all types of trajectories can be described MEE, unlike what occurs if the classical orbit elements are employed. Second, 5 out of 6 equinoctial elements remain constant (while the sixth is integrable) along coast arcs, in the presence of a single attracting body. Third, in the numerical solution of low-thrust path optimization problems, the use of equinoctial elements was proven to mitigate the hypersensitivity issues encountered with spherical coordinates [20,21]. This work considers a specific three-dimensional orbit transfer, already addressed in the scientific literature [11], as a representative example. The main objectives of the present research are thus (i) the implementation and use of IHM for the numerical solution of minimum-fuel orbit transfer problems, (ii) ascertaining the existence of multiple locally optimal solutions, with the consequent identification of the globally optimal transfer, and (iii) investigating the different performance and structures associated with the optimal transfers obtained with different propulsion parameters.

2. Orbit dynamics

This research considers a space vehicle that orbits a single celestial body, in the dynamical framework of the restricted problem of two bodies. The spacecraft of interest is modeled as a point mass. In this research, orbit dynamics is described using MEE.

In general, orbital motion can be described using either Cartesian coordinates, spherical variables, or osculating orbit elements, i.e. semimajor axis a, eccentricity e, inclination i, right ascension of the ascending node (RAAN) Ω, argument of periapsis ω, and true anomaly θ_*. However, the Gauss equations, which govern the time evolution of the orbit elements, become singular in the presence of a circular or equatorial orbit (and also when an elliptic orbit transitions to a hyperbola). For these reasons, MEE [22] are selected in this work as the variables that identify the dynamical state of the space vehicle. These elements are defined as [22]

$$x_1 = a\left(1-e^2\right) \qquad x_2 = e\cos\left(\Omega+\omega\right) \qquad x_3 = e\sin\left(\Omega+\omega\right) \tag{1}$$

$$x_4 = \tan\frac{i}{2}\cos\Omega \qquad x_5 = \tan\frac{i}{2}\sin\Omega \qquad x_6 = \Omega+\omega+\theta_* \tag{2}$$

It is straightforward to recognize that x_1 represents the orbit semilatus rectum. Unlike the classical orbit elements, MEE are never singular, with the only exception of $i = \pi$ (condition that is unlikely to encounter, because equatorial retrograde orbits are rather impractical). If $\eta := 1 + x_2\cos x_6 + x_3\sin x_6$, the instantaneous radius is $r = x_1/\eta$. The classical orbit elements can be retrieved by inverting Eqs. (1)-(2). The spacecraft position can be written in terms of a, e, i, Ω, ω, θ_* or can be computed directly from the equinoctial elements.

The dynamical evolution of the MEE is governed by the respective Gauss equations [22], which can be rewritten in matrix form [23]. Letting $x_6 \equiv q$ and $\boldsymbol{z} := \begin{bmatrix} x_1 & x_2 & x_3 & x_4 & x_5 \end{bmatrix}^T \equiv \begin{bmatrix} p & l & m & n & s \end{bmatrix}^T$, the equations for the MEE are

$$\dot{\boldsymbol{z}} = \mathbf{G}\left(\boldsymbol{z}, x_6\right)\boldsymbol{a} \tag{3}$$

$$\dot{x}_6 = \sqrt{\frac{\mu}{x_1^3}}\eta^2 + \sqrt{\frac{x_1}{\mu}}\frac{x_4\sin x_6 - x_5\cos x_6}{\eta}a_{T,h} \tag{4}$$

DOI: 10.13009/EUCASS2022-6065

where $\boldsymbol{a} \coloneqq \begin{bmatrix} a_{T,r} & a_{T,\theta} & a_{T,h} \end{bmatrix}^T$ is the non-Keplerian acceleration in the local vertical local horizontal (LVLH) frame aligned with $\{\hat{r}, \hat{\theta}, \hat{h}\}$, where unit vector $\hat{r}$ is directed toward the instantaneous position vector $\boldsymbol{r}$ (taken from the center of the attracting body), whereas $\hat{h}$ is aligned with the spacecraft angular momentum. Moreover,

$$\mathbf{G}(\mathbf{z}, x_6) = \sqrt{\frac{x_1}{\mu}} \begin{bmatrix} 0 & \dfrac{2x_1}{\eta} & 0 \\ \sin x_6 & \dfrac{(\eta+1)\cos x_6 + x_2}{\eta} & -\dfrac{x_4 \sin x_6 - x_5 \cos x_6}{\eta} x_3 \\ -\cos x_6 & \dfrac{(\eta+1)\sin x_6 + x_3}{\eta} & \dfrac{x_4 \sin x_6 - x_5 \cos x_6}{\eta} x_2 \\ 0 & 0 & \dfrac{1+x_4^2+x_5^2}{2\eta}\cos x_6 \\ 0 & 0 & \dfrac{1+x_4^2+x_5^2}{2\eta}\sin x_6 \end{bmatrix} \tag{5}$$

where μ is the gravitational parameter of the attracting body. MEE allow identifying the instantaneous position and velocity of the spacecraft. This is controlled using the thrust supplied by the propulsion system. Let T_{max} and m_0 represent the maximum available thrust magnitude and the initial mass of the space vehicle. If x_7 denotes the mass ratio (m/m_0) and T the thrust magnitude, for x_7 the following equation can be obtained:

$$\dot{x}_7 \coloneqq -\frac{\dot{m}}{m_0} = -\frac{u_T}{c} \quad \text{with} \quad 0 \le u_T \le u_T^{(max)} \left(u_T \coloneqq \frac{T}{m_0}, \;\; u_T^{(max)} \coloneqq \frac{T_{max}}{m_0} \right) \tag{6}$$

where c represents the (constant) effective exhaust velocity of the propulsion system, whereas m is the instantaneous mass. The magnitude of the instantaneous thrust acceleration is $a_T = u_T m/m_0 = u_T/x_7$ and is constrained to the interval $0 \le a_T \le a_T^{(max)}$, where $a_T^{(max)} = u_T^{(max)}/x_7$. The thrust acceleration is assumed to be the only non-Keplerian contribution in Eqs. (3)-(5), thus $\boldsymbol{a_T} = \boldsymbol{T}/m = \boldsymbol{T}/(m_0 x_7) = \boldsymbol{u_T}/x_7$. The thrust direction is identified by means of the two thrust angles α ($-\pi \le \alpha \le \pi$) and β ($-\pi/2 \le \beta \le \pi/2$),

$$\boldsymbol{a_T} = \begin{bmatrix} a_r & a_\theta & a_h \end{bmatrix}^T = \frac{u_T}{x_7} \begin{bmatrix} \sin\alpha\cos\beta & \cos\alpha\cos\beta & \sin\beta \end{bmatrix}^T \tag{7}$$

In the end, the spacecraft dynamics is described using the state vector $\boldsymbol{x}$ and the control vector $\boldsymbol{u}$ defined as

$$\boldsymbol{x} \coloneqq \begin{bmatrix} x_1 & x_2 & x_3 & x_4 & x_5 & x_6 & x_7 \end{bmatrix}^T \text{ and } \boldsymbol{u} \coloneqq \begin{bmatrix} u_T & \alpha & \beta \end{bmatrix}^T \tag{8}$$

In light of Eq. (8), Eqs. (3)-(5) can be written in compact form as

$$\dot{\boldsymbol{x}} = \boldsymbol{f}(\boldsymbol{x}, \boldsymbol{u}, t) \tag{9}$$

3. Minimum-fuel orbit transfers

In most mission scenarios of practical interest, spacecraft are equipped with a finite thrust propulsion system. In these dynamical contexts, the crucial objective consists in minimizing propellant consumption. Previous (and rather extensive) works proved that minimum-fuel trajectories include relatively short finite-thrust arcs and long-duration coast intervals [10,24]. This section considers the problem of minimizing the propellant consumption for performing an orbit transfer between two specified (initial and final) orbits, while using MEE to describe the spacecraft dynamics.

DOI: 10.13009/EUCASS2022-6065

3.1 Statement of the problem

The spacecraft of interest is governed by the state equations (9) and is subject to some (problem-dependent) boundary conditions of the form $\boldsymbol{\psi}(\boldsymbol{x_0}, \boldsymbol{x_f}, t_0, t_f) = \boldsymbol{0}$. These conditions usually include the relations that define the initial and final orbits. The initial time t_0 is assumed specified and is set to 0. The objective function $\hat{J}$ to minimize is the propellant mass, and this is equivalent to maximizing the final mass ratio $x_{7,f}$. Thus, for the problem at hand the objective is

$$\hat{J} = -k_J x_{7,f} \tag{10}$$

where $k_J > 0$ is a positive, arbitrary constant. Therefore, the problem consists in finding the optimal control $\boldsymbol{u}$ that minimizes the objective function (10), while holding the state equations (9) and the boundary conditions $\boldsymbol{\psi} = \boldsymbol{0}$.

3.2 Necessary conditions for optimality

In order to derive the necessary conditions for optimality, a Hamiltonian function H and a function Φ are defined as

$$H \coloneqq \boldsymbol{\lambda}^{\boldsymbol{T}} \boldsymbol{f}(\boldsymbol{x}, \boldsymbol{u}, t) \qquad \Phi \coloneqq -k_J x_{7,f} + \boldsymbol{\nu}^{\boldsymbol{T}} \boldsymbol{\psi}(\boldsymbol{x}_0, \boldsymbol{x}_{\boldsymbol{f}}, t_0, t_f) \tag{11}$$

where $\boldsymbol{\lambda}$ is the adjoint vector associated with the state equations, $\boldsymbol{\nu}$ is the vector of the (time-independent) adjoint variables conjugate to the boundary conditions. The following necessary conditions for optimality are obtained from the first differential of the extended objective function [25]:

$$\boldsymbol{\lambda}_0 + \left(\frac{\partial \Phi}{\partial \boldsymbol{x}_0}\right)^T = 0 \rightarrow \boldsymbol{\lambda}_0 = -\left(\frac{\partial \boldsymbol{\psi}}{\partial \boldsymbol{x}_0}\right)^T \boldsymbol{\nu} \tag{12}$$

$$\boldsymbol{\lambda}_{\boldsymbol{f}} - \left(\frac{\partial \Phi}{\partial \boldsymbol{x}_{\boldsymbol{f}}}\right)^T = 0 \rightarrow \boldsymbol{\lambda}_{\boldsymbol{f}} = \left(\frac{\partial \boldsymbol{\psi}}{\partial \boldsymbol{x}_{\boldsymbol{f}}}\right)^T \boldsymbol{\nu} \tag{13}$$

$$H_f + \frac{\partial \Phi}{\partial t_f} = 0 \rightarrow H_f = -\left(\frac{\partial \boldsymbol{\psi}}{\partial t_f}\right)^T \boldsymbol{\nu} \tag{14}$$

$$\dot{\boldsymbol{\lambda}} = -\left(\frac{\partial H}{\partial \boldsymbol{x}}\right)^T \tag{15}$$

$$\boldsymbol{u}^* = \arg\min_{\boldsymbol{u}} H \tag{16}$$

The last condition represents the Pontryagin minimum principle [26], with subscript * denoting the optimal value of the corresponding variable. Equation (15) is the adjoint equation for the costate vector, accompanied by the related boundary conditions (12) and (13). Because $\boldsymbol{\psi}$ appears in Eqs. (12) and (13), their explicit form is problem-dependent. Furthermore, Eq. (14) holds for the final value of the Hamiltonian function.

Using Eqs. (3)-(5) and (11), H can be rewritten as

$$H = \frac{u_T}{x_7}\left[H_r(\boldsymbol{y}, \boldsymbol{\lambda})\cos\beta\cos\alpha + H_\theta(\boldsymbol{y}, \boldsymbol{\lambda})\cos\beta\sin\alpha + H_h(\boldsymbol{y}, \boldsymbol{\lambda})\sin\beta - \lambda_7 \frac{x_7}{c}\right] + H_0(\boldsymbol{y}, \boldsymbol{\lambda}) \tag{17}$$

where $\boldsymbol{y}$ collects components x_1 through x_6 of the state, i.e. $\boldsymbol{y} \coloneqq [x_1 \;\; x_2 \;\; x_3 \;\; x_4 \;\; x_5 \;\; x_6]^T$. Due to Eq. (15), the adjoint equation for λ_7 is

$$\dot{\lambda}_7 = -\frac{\partial H}{\partial x_7} = \frac{H_r(\boldsymbol{y}, \boldsymbol{\lambda})\cos\beta\cos\alpha + H_\theta(\boldsymbol{y}, \boldsymbol{\lambda})\cos\beta\sin\alpha + H_h(\boldsymbol{y}, \boldsymbol{\lambda})\sin\beta}{x_7^2} \tag{18}$$

DOI: 10.13009/EUCASS2022-6065

Moreover, because the final mass is unspecified (and in fact is to be minimized), the boundary conditions are independent of $x_{7,f}$. As a result, Eq. (13) yields

$$\lambda_{7,f} = -k_J < 0 \tag{19}$$

Arbitrariness of constant k_J allows obtaining an inequality condition in place of an equality condition. Moreover, the minimum principle (16) allows expressing the optimal control in terms of the state and costate variables. With reference to Eq. (17), the first three terms in square parentheses can be regarded as a dot product. Thus, since $u_T/x_7 > 0$, the thrust angles that minimize H are given by

$$\begin{cases} \sin\alpha = -\dfrac{H_r\left(H_r^2+H_\theta^2+H_h^2\right)^{-1/2}}{\cos\beta} = -H_r\left(H_r^2+H_\theta^2\right)^{-1/2} \\ \cos\alpha = -\dfrac{H_\theta\left(H_r^2+H_\theta^2+H_h^2\right)^{-1/2}}{\cos\beta} = -H_\theta\left(H_r^2+H_\theta^2\right)^{-1/2} \end{cases} \quad , \ \alpha \in [-\pi, \pi[\tag{20}$$

$$\sin\beta = -H_h\left(H_r^2+H_\theta^2+H_h^2\right)^{-1/2} , \quad \beta \in \left[-\frac{\pi}{2}, \frac{\pi}{2}\right] \tag{21}$$

Using these expressions for H and λ_7, Eqs. (17) and (18) become

$$H = \tilde{H} - u_T\left[\frac{1}{x_7}\left(H_r^2+H_\theta^2+H_h^2\right)^{1/2} + \frac{\lambda_7}{c}\right] \tag{22}$$

$$\dot{\lambda}_7 = -\frac{u_T}{x_7^2}\left(H_r^2+H_\theta^2+H_h^2\right)^{1/2} \le 0 \tag{23}$$

The latter relation, in conjunction with the final condition (19), implies that λ_7 cannot be positive at all times. Moreover, using the Pontryagin minimum principle and Eq. (22), the optimal value of u_T is

$$u_T = \begin{cases} u_T^{(max)} & \text{if } S > 0 \\ 0 & \text{if } S < 0 \end{cases} \quad \text{with} \quad S := \frac{\sqrt{H_r^2+H_\theta^2+H_h^2}}{x_7} + \frac{\lambda_7}{c} \tag{24}$$

This means that a minimum-fuel path includes powered phases (where the maximum available thrust is used) and coast arcs. In the previous relation, S is referred to as the switching function, because it determines the switching times between the two arc types that compose the optimal trajectory. Equation (24) is obtained under the assumption of neglecting singular arcs, associated with the condition $S \equiv 0$ over a time interval of finite duration. The existence of similar arcs can be investigated using singular optimal control theory [27]. It is worth stressing that the existence of coast arcs and powered phases along minimum-fuel space trajectories was already proven using different representations for the dynamical state (e.g., Cartesian or spherical coordinates [18,19,28]). Therefore, the previous analytical developments, already reported in [18], represent an alternative derivation leading to an expected result.

In the end, the necessary conditions for optimality, in conjunction with the state equations (9) and the boundary conditions, allow converting the original optimal control problem into a two-point boundary-value problem, where the unknowns are the state $\boldsymbol{x}$, the control $\boldsymbol{u}$, the final time t_f, and the adjoint variables $\boldsymbol{\lambda}$ and $\boldsymbol{\nu}$.

4. Indirect heuristic method

The Indirect Heuristic Method (IHM) is based on the joint use of the necessary conditions for optimality and a heuristic algorithm. The Pontryagin minimum principle allows expressing the control variables in terms of the state and the costate (cf. Eqs. (20) and (21)). As a result, the unknown parameters are the initial values of the adjoint variables, together with the final time and, possibly, some initial state conditions. The heuristic algorithm (differential evolution in this research) uses a population of individuals; each of them corresponds to a particular selection of the unknown parameters. Then, the population is expected to evolve to include the fittest individual, which corresponds to the optimal solution to the problem of interest.

DOI: 10.13009/EUCASS2022-6065

4.1 Algorithm structure

The starting point of the method is the definition of the necessary conditions for optimality, illustrated in Section 3. All of these must be enforced, in particular the adjoints equations (15). Based on these and the equations of motion, two preliminary steps are completed:

(a) define the known initial values of the state and costate using the boundary conditions ($\boldsymbol{\psi} = \mathbf{0}$) and the necessary condition (12);
(b) with the use of Eq. (12), determine the existence of relations among the initial values of the state and the costate, and eliminate the corresponding components of the vector $\boldsymbol{\nu}$ of time-independent multipliers.

Then, for each individual the numerical solution process involves the following steps:

(c) identify the unknown initial values of the costate, and select a value for each of them;
(d) select a value of the final time t_f;
(e) as long as the current time $t < t_f$, identify the type of trajectory arc (either powered or ballistic), using Eq. (24), and integrate the equations of motion (9) and the adjoints equations (15) until the switching function changes its sign or $t = t_f$;
(f) if $t < t_f$, repeat step (e);
(g) evaluate the boundary conditions violations at t_f and the necessary conditions (13) and (14) on the final state, costate, and Hamiltonian, and evaluate the auxiliary objective function J_{mod} (cf. Section 5); if inequality (19) is violated, then set J_{mod} to a predefined, very large value;

When the value of J_{mod} of the best individual does not exceed a prescribed tolerance, then convergence is declared, and the algorithm stops, otherwise a new generation is created (cf. Section 4.2) and steps (c) through (g) are repeated for each individual.

A major difficulty is the identification of the switching times, which determine the thrust sequence. High numerical accuracy is needed for the identification of these times, and numerical integration must stop and restart at every sign change of the switching function. In this work, the *MATLAB* function *ODE Event Location* was used, and the sign changes of S are detected with a precision set to 10^{-15} during the numerical integration.

It is worth remarking that the scalability property of multipliers [20] allows defining their search space as $[\lambda_{min},\ \lambda_{max}]$, with $\lambda_{min} < 0$ and $\lambda_{max} > 0$.

4.2 Differential evolution

The algorithm termed Differential Evolution (DE) is used as the heuristic approach. It was introduced by Storn and Price [17,29] in 1995. It belongs to the class of evolutionary algorithms and is based on the creation of a population of individuals that is randomly initialized in the first iteration of the method. From this first population the next ones are generated by the algorithm.

A population is composed of N individuals, while the vector size of the unknown parameters is n. A typical choice that usually ensures convergence is $N \geq 10n$. Each individual represents a possible solution to the problem and is used to evaluate the auxiliary objective function J_{mod}. At the end of the iterative process, the individual associated with the minimum value of the objective function is declared as the solution. The generation of a population of individuals occurs by "perturbing" the individuals of the previous population. The vector of unknown parameters is defined as

$$\boldsymbol{\chi} = \left[\chi_1, \ldots, \chi_n\right]^T \tag{25}$$

The evolution of the dynamic system depends on these parameters. Each element of the vector $\boldsymbol{\chi}$ has its specific search space, i.e.

$$a_k \leq \chi_k \leq b_k \quad (k = 1, \ldots, n) \tag{26}$$

If a parameter exceeds the lower or upper bound of the search space, it is set to the limiting value (either its upper bound or its lower bound). Each individual corresponds to a vector $\boldsymbol{\chi}(i) = [\chi_1(i),\ \ldots,\ \chi_n(i)]^T$ with $i = 1, \ldots, N$, and is associated with a value of the objective function. The initial population is defined randomly by introducing N individuals, with parameters generated stochastically and uniformly distributed in their search space given by Eq. (26). The DE algorithm consists of four steps, to be performed at each iteration j. All details can be found in the references [17,29]. In each iteration j, for the generic individual i (i = 1,…,N), the following steps are completed:

DOI: 10.13009/EUCASS2022-6065

1. Evaluate the objective function $J_{mod,i}^{(j)}$ associated with parameter vector $\boldsymbol{\chi}(i)$ (termed *target* vector).
2. *Mutation* phase. With the exception of the best individual (not subject to mutation), select 2 random integers $q, r \in [1,..., N]$, with $q, r \neq i$, then generate a mutant parameter vector $\boldsymbol{\psi}(i)$ $\left(:=\left[\psi_1(i) \ \ldots \ \psi_n(i)\right]^T\right)$,

$$\boldsymbol{\psi}(i) = \boldsymbol{\chi}\left(i_{opt}\right) + F\left(\boldsymbol{\chi}(q) - \boldsymbol{\chi}(r)\right) \tag{27}$$

where $\boldsymbol{\chi}\left(i_{opt}\right)$ is the current best individual. The mutant parameter vector $\boldsymbol{\psi}(i)$ is generated by adding the weighted difference between two parameter vectors (indices *q* and *r*) to the *base* parameter vector $\boldsymbol{\chi}\left(i_{opt}\right)$. $F \in [0,\ 2]$ is a real valued constant referred to as *differential weight*, which controls the amplification of the differential term.

3. *Crossover* phase. Select a random integer $\zeta \in [1,\ n]$. Initialize $\boldsymbol{Y}(i) = \boldsymbol{\chi}(i)$, $k = \zeta$ and $L = 1$. While rand(0,1) < *CR* and $L < n$
   (a) $Y_k(i) = \psi_k(i)$
   (b) if $(\zeta + L) \leq n$ then $k = \zeta + L$ else $k = \zeta + L - n$
   (c) $L = L + 1$
   $CR \in [0,1]$ is the crossover constant, whereas rand(0,1) is an independent random variable, with uniform distribution in [0,1].
4. *Selection* phase. Evaluate the objective function $J_{T,mod,i}^{(j)}$ associated with the trial parameter vector $\boldsymbol{Y}(i)$. Select the parameter vector $\boldsymbol{\chi}^{(j+1)}(i)$ using

$$\boldsymbol{\chi}^{(j+1)}(i) = \begin{cases} \boldsymbol{\chi}(i) \text{ if } & J_{mod,i}^{(j)} < J_{T,mod,i}^{(j)} \\ \boldsymbol{Y}(i) \text{ if } & J_{mod,i}^{(j)} > J_{T,mod,i}^{(j)} \end{cases} \tag{28}$$

At each iteration, index i of the individual that corresponds to the minimum value of the objective function among those obtained by the entire population is set aside and, at the end of the search, the best individual is the one that corresponds to the global minimum of the objective function J_{mod}. The process ends when either the maximum number of generations N_{iter} is reached, or J_{mod} is less than a specified threshold value, or the phenomenon of stagnation occurs. Several versions of the algorithm exist. The one used in this work is the $DE/best/1/exp$, which is the default version for the DE implementation in *MATLAB*, programmed by Buehren [30].

DE can be also used as the initial numerical method for finding an approximate solution to the problem of interest. Further search can be carried out with local optimizers, such as $fminsearch$ in *MATLAB*, which can be used for final refinement of the solution. In this research, DE was used both as a standalone method and as a preprocessing technique. In the latter case, DE was stopped when $J_{mod} < 10^{-3}$. As a rule of thumb, however, the maximum number of iterations must be a priori set to a large value, in all runs of DE. Table 1 reports the parameters used for implementing and running DE.

Table 1: DE settings

N	100
F	0.8
CR	0.7

DOI: 10.13009/EUCASS2022-6065

5. Test case: three-dimensional Earth orbit transfer

The problem of determining the minimum-fuel path between two specific Earth orbits is considered as an illustrative example, taken from the scientific literature [19]. The initial and final orbit elements are reported in Table 2. The true anomaly is unspecified along both the initial and the final orbit. As a result, the vector related to the final conditions is

$$\boldsymbol{\psi} = \begin{bmatrix} x_{1,f} - p_d \\ x_{2,f} - e_d \cos\left(\Omega_d + \omega_d\right) \\ x_{3,f} - e_d \sin\left(\Omega_d + \omega_d\right) \\ x_{4,f} - \tan\left(i_d/2\right)\cos\Omega_d \\ x_{5,f} - \tan\left(i_d/2\right)\sin\Omega_d \end{bmatrix} \tag{29}$$

where $p_d = a_d\left(1-e_d^2\right)$. Trajectory optimization was performed several times, with the intent of retrieving the solution reported in the literature, but also for the purpose of ascertaining the existence of alternate locally optimal transfers. The necessary conditions for optimality yield $\lambda_{6,f} = 0$ and $H_f = 0$, because Φ is independent of $x_{6,f}$ and t_f.

Canonical units are used in the numerical solution process. The distance unit (DU) equals the Earth radius (1 DU $= R_E = 6378.136$ km) whereas the time unit (TU) is such that the Earth gravitational parameter $\mu = 1$ DU$^3/TU^2$; this leads to 1 TU $= 806.8$ s. The orbit elements of the initial and final orbit are reported in Table 2. Because the initial and final values of x_6 are unspecified, from Eqs. (12) one obtains $\lambda_{6,0} = \lambda_{6,f} = 0$. Hence, for the problem at hand the parameter set is given by $\boldsymbol{\chi} = \begin{bmatrix} \lambda_{1,0} & \lambda_{2,0} & \lambda_{3,0} & \lambda_{4,0} & \lambda_{5,0} & \lambda_{7,0} & x_{6,0} & t_f \end{bmatrix}^T$. In all cases, a reasonable choice was found to be the interval $[-10,10]$ for $\lambda_{7,0}$ and $[-1,1]$ for the remaining adjoint variables. The search space for the initial state variable $x_{6,0}$ is $[-\pi,\pi]$, whereas t_f was sought in different intervals, depending on each specific case (cf. Sections 5.1 through 5.3).

Table 2: Initial and final orbit elements

	Initial	Final
a_d [km]	6571.004	10 000
e_d	0.01	0
i_d [deg]	1	65
ω_d [deg]	10	/
Ω_d [deg]	30	30

5.1 Reference solution from previous research

Using the data reported in [19], fundamental spacecraft parameters are

$$c = 3922.6 \text{ m/s}; \quad T = 1000 \text{ N}; \quad m_0 = 3000 \text{ kg}; \quad u_T^{(max)} = 3.3310^{-1} \text{ m/s}^2 = 3.3910^{-2}\, g_0 \tag{30}$$

where m_0 denotes the initial mass, T the maximum thrust, whereas g_0 is the gravitational acceleration at sea level. The search space for the time of flight is set to [10000, 25000] sec. For the problem at hand, the auxiliary objective function J_{mod} is defined as

DOI: 10.13009/EUCASS2022-6065

$$J_{mod} = \left\| \begin{bmatrix} \boldsymbol{\psi} \\ \lambda_{6,f} \\ \dfrac{H_f}{std\left\{\left|\lambda_{1,f}\right|,\left|\lambda_{2,f}\right|,\left|\lambda_{3,f}\right|,\left|\lambda_{4,f}\right|,\left|\lambda_{5,f}\right|,\left|\lambda_{6,f}\right|\right\}} \end{bmatrix} \right\| \tag{31}$$

The last line reports the standard deviation on the final values of the adjoint variables, and is aimed at preventing H_f from vanishing due to modest values of all these final values. The maximum number of iterations N_{iter} was set to 3000, and the process was stopped after 1745 iterations, at the first occurrence of the condition $J_{mod} < 10^{-3}$.

Table 3 reports some fundamental quantities related to the numerical results. The transfer trajectory, the switching function and the optimal thrust angles are shown in Figs. 1-4. In all the figures the red color denotes powered phases, while the blue color corresponds to coast arcs.

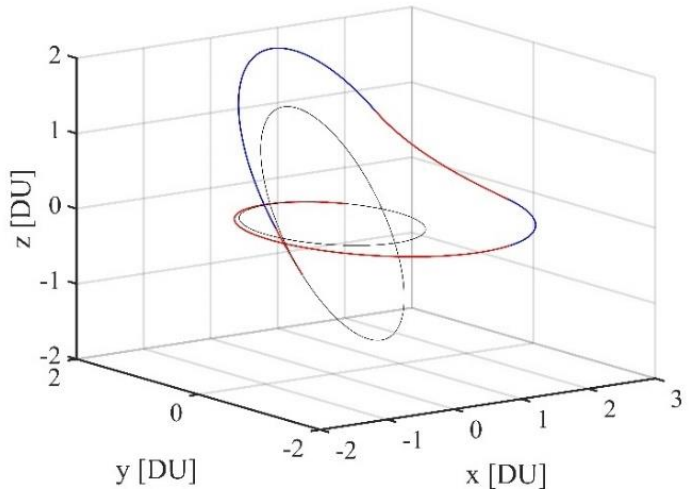

Figure 1: transfer trajectory (reference solution)

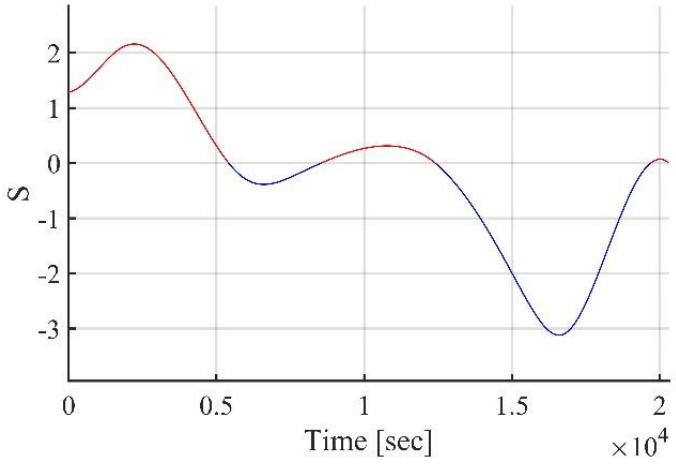

Figure 2: switching function (reference solution)

DOI: 10.13009/EUCASS2022-6065

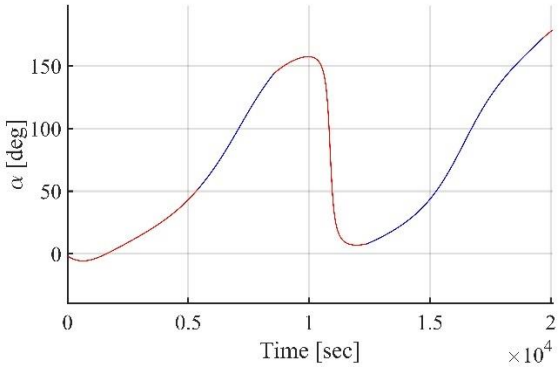

Figure 3: thrust angle α (reference solution)

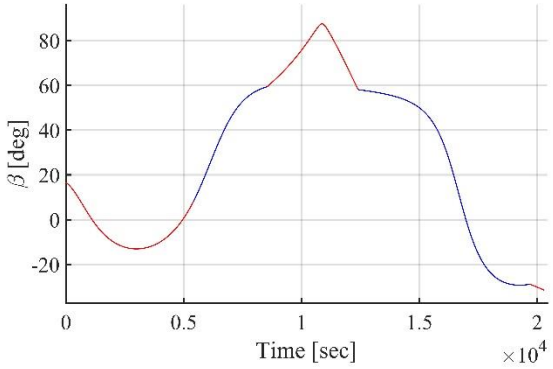

Figure 4: thrust angle β (reference solution)

Table 3: Summary of main numerical results (reference solution)

t_f [s]	20 294
$x_{7,f}$	0.159
H_f	o(10^{-11})

5.2 Globally optimal solution

The same data (i.e. propulsion parameters and initial and final orbit elements) were used again, while adopting the definition of the modified objective function J_{mod} reported in Eq. (31). On the other hand, the search interval of the transfer time was changed to [20000, 40000] s. The parameter N_{iter} was set to 3000 again, and the process was stopped after 1672 iterations, at the first occurrence of the condition $J_{mod} < 10^{-3}$.

The main results are reported in Table 4. The transfer trajectory, the switching function and the optimal thrust angles are shown in Figs. 5-8.

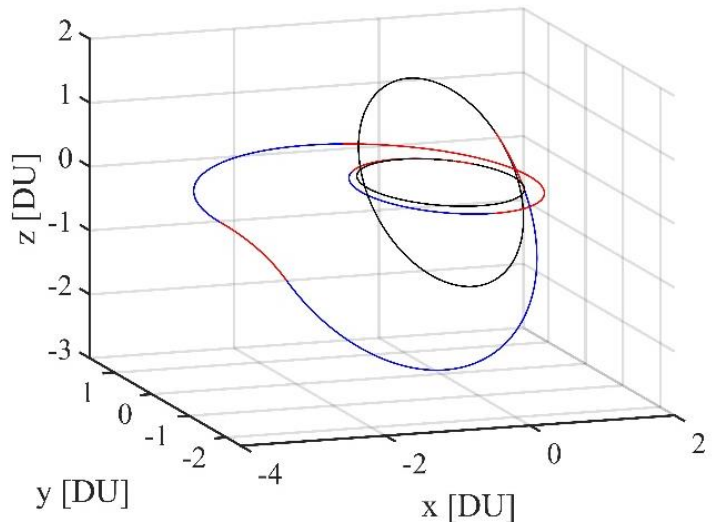

Figure 5: Globally optimal transfer trajectory

DOI: 10.13009/EUCASS2022-6065

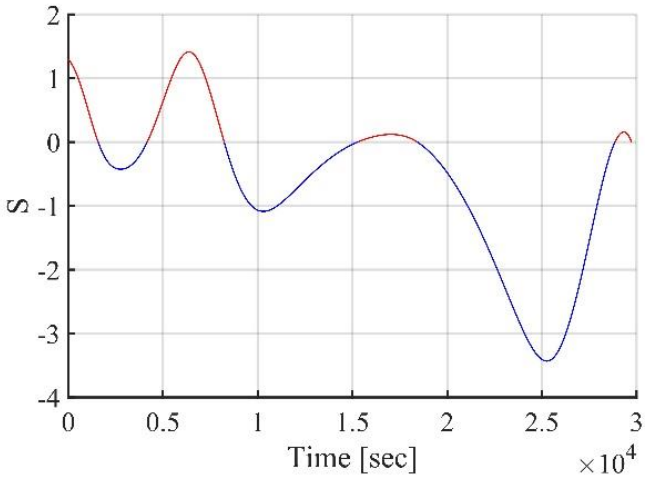

Figure 6: switching function (globally optimal solution)

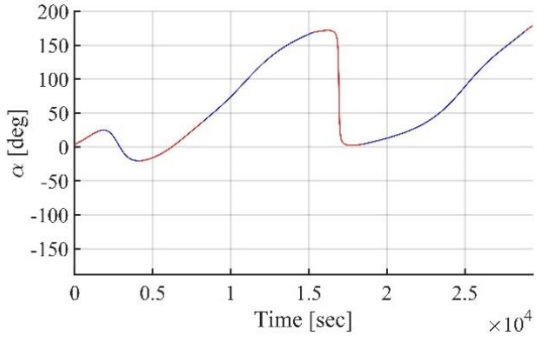

Figure 7: thrust angle α (globally optimal solution)

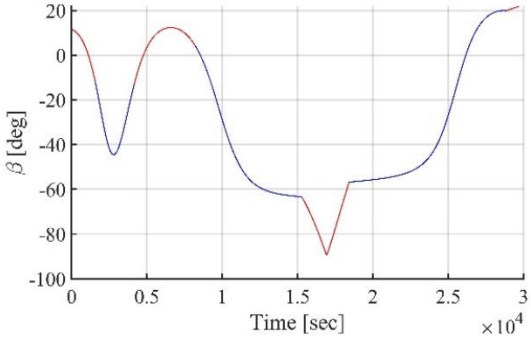

Figure 8: thrust angle β (globally optimal solution)

Table 4: Summary of main numerical results (globally optimal solution)

t_f [s]	29 729
$x_{7,f}$	0.179
H_f	o(10^{-11})

It is interesting to compare the trajectory shown in Figure 5 with the impulsive solution reported in [19]. It is evident the similarity between the structures of the two trajectories. However, it is worth noting that the finite-thrust solution involves an additional orbit around the Earth, and the optimal path shown in Figure 5 is a three-elliptic orbit transfer as a result. This solution is associated with higher final mass ratio and therefore lower propellant consumption than the solution shown in section 5.1 and reported in scientific literature [19].

The solution found in this research can be considered globally optimal with an upper bound on the time of flight set to 40000 sec, and corresponds to $x_{7,f} = 0.179$ and $t_f = 29729$ s. For comparison, the impulsive solution [19] yields $x_{7,f} = 0.194$ and $t_f = 28540\ s$. However, it is worth remarking that the theoretical, globally optimal impulsive transfer with orbit plane change is the biparabolic one. For the case at hand, the biparabolic transfer yields $x_{7,f} = 0.226$, greater than that obtained in this work (and larger than that of the bielliptic transfer). In the biparabolic (limiting) case the plane change would take place at infinite distance, at no cost, and of course the time of flight would tend to infinity.

DOI: 10.13009/EUCASS2022-6065

5.3 Locally optimal solutions

During the search for the optimal solution to the problem addressed in [19], two locally optimal solutions were detected. These meet the necessary conditions but correspond to higher propellant consumptions. Although less interesting than the preceding solutions, they are remarkable in the fact that they confirm the existence of multiple solutions for minimum-fuel orbit transfers (with an upper bound on the time of flight). The main results are reported in Table 5. For the sake of brevity, only the trajectories are reported for these solutions (cf. Figs. 9-10). It is worth noting that these two locally optimal transfers have different structures, i.e. 6 powered arcs (transfer 3), and a single, continuous powered arc (transfer 4). As a further remark, the final mass ratio reaches modest values (especially for transfer 4), which make these transfers practically infeasible with the current technology.

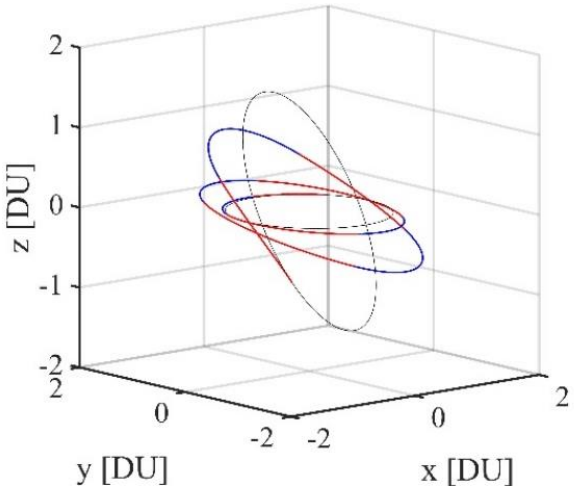

Figure 9: Trajectory, locally optimal solution (transfer 3)

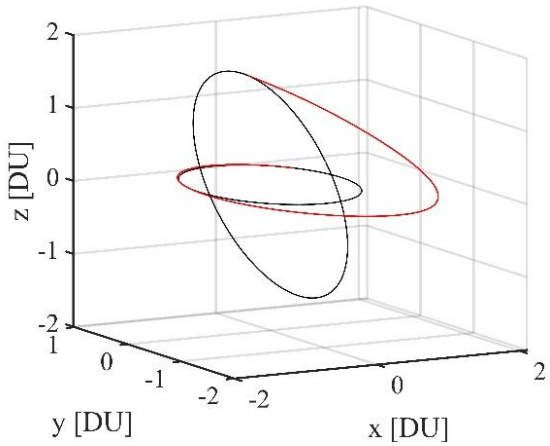

Figure 10: Trajectory, locally optimal solution (transfer 4)

Table 5: Summary of main numerical results (locally optimal solutions)

	Transfer 3	Transfer 4
$t_f\ [s]$	19838	10651
$x_{7,f}$	0.123	9.45 e-2
H_f	o(10^{-4})	o(10^{-4})

DOI: 10.13009/EUCASS2022-6065

5.4 Optimal transfers with different thrust magnitudes

Minimum-fuel transfers between the same terminal orbits were found numerically using different thrust magnitudes, reported in Table 6. For cases 1 and 3, J_{mod} is defined with only H_f as the last element (without introducing the denominator reported in the last element of Eq. (31)). Instead, for case 2, an amended definition of J_{mod} was adopted, with last term given by

$$\frac{100\, H_f}{std\,[|\lambda_{1,f}|,|\lambda_{2,f}|,|\lambda_{3,f}|,|\lambda_{4,f}|,|\lambda_{5,f}|,|\lambda_{7,f}|]^T} \tag{31}$$

The main numerical results are listed in Table 6; N_{it} denotes the number of iterations needed to reach the condition $J_{mod} < 10^{-3}$. For the sake of brevity, only the trajectories are reported for these solutions (cf. Figs.11-13). It is worth noting that for cases 2 and 3 the final mass ratio approaches or is less than 0.1, which implies that the transfers at hand are practically infeasible with the current technological constraints. The final mass ratio increases as thrust magnitude increases, which is consistent with the classical theory of optimal finite-thrust and impulsive transfers [26]. Moreover, these 3 transfers have different structures, i.e. 5 powered arcs (case 1), 9 powered arcs (case 2), and a single, continuous powered arc (case 3).

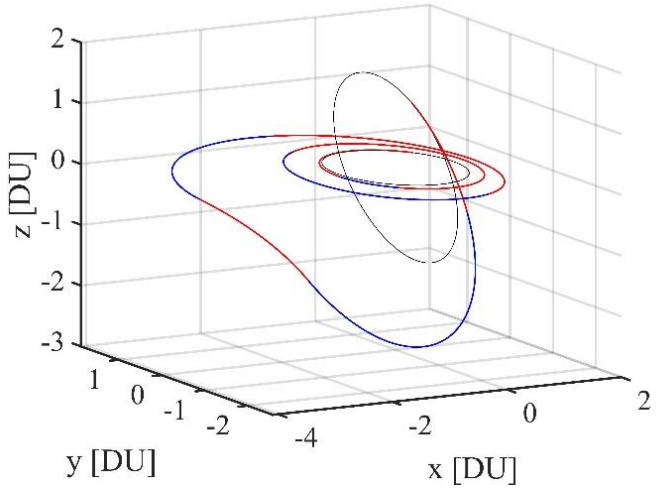

Figure 11: Trajectory, case 1

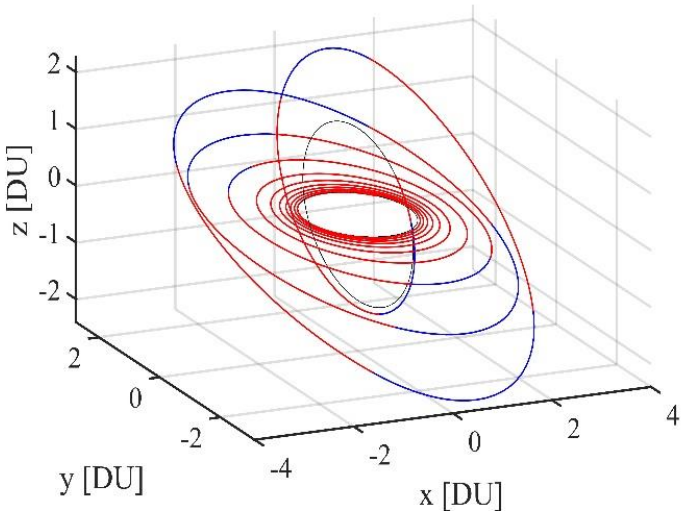

Figure 12: Trajectory, case 2

DOI: 10.13009/EUCASS2022-6065

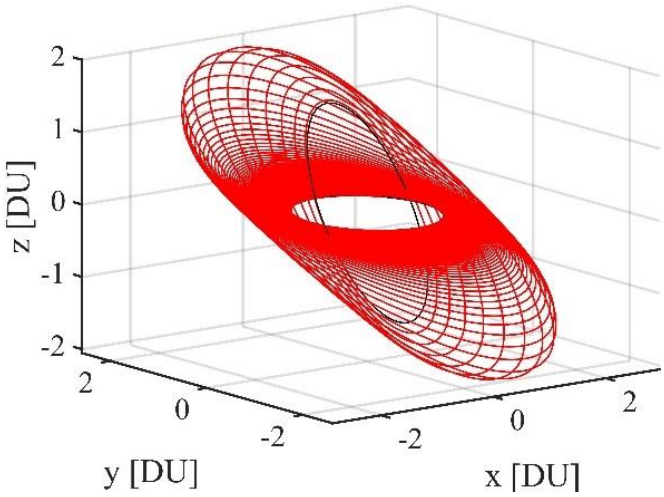

Figure 13: Trajectory, case 3

Table 6: Data and main numerical results for different thrust magnitudes

	Case 1	Case 2	Case 3
T [N]	500	100	10
t_f	42890 s	1.71 days	12.71 days
$x_{7,f}$	0.168	0.101	6.66 e-2
H_f	o(10^{-4})	o(10^{-5})	o(10^{-4})
N_{it}	4143	2215	832

6. Concluding remarks

This research addresses the problem of determining three-dimensional minimum-fuel, finite-thrust orbit transfers, using the indirect heuristic method. This approach was previously introduced and successfully employed for the purpose of finding minimum-time space trajectories, even with eclipse constraints on the available thrust. In this work its use is extended to minimum-fuel orbit transfers. The technique at hand is based upon the joint use of the necessary conditions for optimality and a heuristic algorithm. More specifically, the necessary conditions are employed to express the control variables (i.e., the thrust magnitude and direction) as functions of the adjoint variables, which are subject to the Euler-Lagrange equations. As a result, a reduced parameter set – mainly composed of the unknown initial values of the adjoint variables – suffices to transcribe the optimal control problem into a parameter optimization problem. Furthermore, the optimal control variables are determined without any restriction, because no particular representation is assumed. Lastly, satisfaction of all the analytical conditions provides a clear indication on local optimality of the solution. The indirect heuristic technique is thus capable of circumventing the main shortcomings of using heuristic approaches, while retaining the main advantage, which is the absence of any starting guess. Minimum-fuel paths admit coast arcs and powered phases, whose sequence is unknown a priori and depends on the switching function. This circumstance adds further complexity to the study of minimum-fuel transfers compared to minimum-time trajectories. In this research, minimum-fuel orbit transfers are sought with the use of modified equinoctial elements. An illustrative example taken from the scientific literature is considered, and the known solution is first retrieved. Yet, this work proves the existence of an alternative solution that outperforms the preceding one, together with several further locally optimal solutions, with different sequences of thrust phases and coast arcs. Minimum-fuel orbit transfers are also identified for different values of the propulsion parameters. The numerical results point out the existence of a variety

DOI: 10.13009/EUCASS2022-6065

of structures for the optimal transfer. In fact, different sequences of powered phases and coast arcs are proven to exist, and their number reduces as the thrust magnitude increases. All the optimal paths enjoy the analytical conditions to a great accuracy, and the numerical solution method did not encounter hypersensitivity issues. These circumstances unequivocally testify to the effectiveness and accuracy of the indirect heuristic methodology, with the use of modified equinoctial elements, in detecting minimum-fuel orbit transfers.

References

[1] Hohmann, W. 1925. Die Erreichbarkeit der Himmelskoerper, Oldenbourg, Munich; also NASA Translation TT–F–44. 1960. The Attainability of Heavenly Bodies.
[2] Bliss, G.A. 1946. Lectures on the Calculus of Variations. University of Chicago Press, Chicago. 108–112.
[3] Leitmann, G. 1956. A calculus of variations solution of Goddard's problem, *Astronautica Acta* 2: 55–62.
[4] Cicala, P. 1957. An Engineering Approach to the Calculus of Variations. Levrotto & Bella, Torino.
[5] Bellman, R. 1957. Dynamic Programming. Princeton University Press, Princeton.
[6] Miele, A. 1958. General variational theory of the flight paths of Rocket–Powered aircraft, missiles, and satellite carriers, *Astronautica Acta* 4: 11–21.
[7] Pontryagin, L.S., Boltyanskii, V.G., Gamkrelidze, R.V., and Mishchenko, E.F. 1962. The Mathematical Theory of Optimal Processes. Princeton University Press, New York.
[8] Bryson, A.E., and Ho, Y.C. 1969. Applied Optimal Control. Ginn and Company, Waltham.
[9] Vinh, N.X. 1973. General theory of optimal trajectory for rocket flight in a resisting medium. *Journal of Optimization Theory and Applications* 11: 189–202.
[10] Lawden, D.F. 1963. Optimal Trajectories for Space Navigation, Butterworths, London, U. K.
[11] Robbins, H.M. 1966. An Analytical Study of the Impulsive Approximation. *AIAA Journal* 4 (8):1417-1423.
[12] Taheri, E., and Junkins, J.L. 2020. How Many Impulses Redux. *The Journal of the Astronautical Sciences* 67: 257-334.
[13] Betts, J.T. 1988. Survey of Numerical Methods for Trajectory Optimization. *Journal of Guidance, Control, and Dynamics* 21 (2): 193-207.
[14] Conway, B.A. 2012. A Survey of Methods Available for the Numerical Optimization of Continuous Dynamical Systems. *Journal of Optimization Theory and Applications* 152: 271-306.
[15] Pontani, M., and Conway, B.A. 2014. Optimal Low-Thrust Orbital Maneuvers via Indirect Swarming Method. *Journal of Optimization Theory and Application* 162:272-292.
[16] Pontani, M., and Conway, B.A. 2015. Minimum-Fuel Finite-Thrust Relative Orbit Maneuvers via Indirect Heuristic Method. *Journal of Guidance, Control, and Dynamics* 38:913-924.
[17] Storn, R., and Price, K. 1997. Differential Evolution – A Simple and Efficient Heuristic for Global Optimization over Continuous Spaces. *Journal of Global Optimization* 11:341–359.
[18] Pontani, M. 2021. Optimal Space Trajectories with Multiple Coast Arcs Using Modified Equinoctial Eléments. *Journal of Optimization Theory and Application*. 191: 545-574.
[19] Pan, B., Lu, P., and Chen, Z. 2012. Three-dimensional closed-form costate solutions in optimal coast. *Acta Astronautica* 77:156–166.
[20] Pontani, M. 2020. Optimal Low-Thrust Trajectories Using Nonsingular Equinoctial Orbit Elements. *Advances in the Astronautical Sciences* 170: 443-462.
[21] Singh, S. K., Taheri, E., Woollands R., and Junkins, J.L. 2019. Mission Design for Close-Range Lunar Mapping by Quasi-Frozen Orbits. In: *70th International Astronautical Congress*. IAC-19-C1.1.11.
[22] Battin, R.H. 1987. An Introduction to the Mathematics and Methods of Astrodynamics. AIAA Education Series, New York. 448–450, 490–494.
[23] Pontani, M., and Corallo, F. 2021. Optimal Low-Thrust Orbit Transfers With Shadowing Effect Using A Multiple-Arc Formulation. In: *72th International Astronautical Congress.* IAC-21-C1.5.12.
[24] Prussing, J.E. 2001. Primer Vector Theory and Applications. In: Conway, B. (ed.) Spacecraft Trajectory Optimization. Cambridge University Press. New York. 16-36.
[25] Hull, D.G. 2003. Optimal Control Theory for Applications. Springer International Edition. New York. 95-100. 142-143. 221-223.
[26] Longuski, J.M., Guzman, J.J. and Prussing, J.E. 2014. Optimal Control with Aerospace Applications. Springer. New York.
[27] Bell, D.J., and Jacobson, D.H. 1975. Singular Optimal Control Problems. Academic Press. New York. 1-100.
[28] Glandorf, D.R. 1968. Lagrange multipliers and the state transition matrix for coasting arcs. *AIAA J.* 7:363–365.
[29] Storn, R., and Price, K. 1995. Differential Evolution – A Simple and Efficient Adaptive Scheme for Global Optimization Over Continuous Spaces. International Computer Science Institute. TR-95-012.
[30] Bueheren, M., https://www.mathworks.com/matlabcentral/fileexchange/18593-differentialevolution, MATLAB Central File Exchange, accessed on April 3, 2021.